Targeted reprogramming of H3K27me3 resets epigenetic memory in plant paternal chromatin

Michael Borg [1], Yannick Jacob [2,3], Daichi Susaki [4], Chantal LeBlanc [3], Daniel Buend€a[1], Elin Axelsson [1], Tomokazu Kawashima [1,5], Philipp Voigt [6], Leonor Boavida [7,8], J•rg Becker [7], Tetsuya Higashiyama [4,9], Robert Martienssen [2], Fr,d,ric Berger [1,*]

[1]Gregor Mendel Institute, Austrian Academy of Sciences, Vienna BioCenter, Dr. Bohr-Gasse 3, 1030 Vienna, Austria

[2]Howard Hughes Medical Institute-Gordon and Betty Moore Foundation, Watson School of Biological Sciences, Cold Spring Harbor Laboratory, New York 11724, USA

[3]Yale University, Department of Molecular, Cellular and Developmental Biology, Faculty of Arts and Sciences, 219 Prospect Street, New Haven, Connecticut 06511, USA

[4]Graduate School of Science, Nagoya University, Furo-cho, Chikusa-ku, Nagoya, 464-8601 Aichi, Japan

[5]Department of Plant and Soil Sciences, University of Kentucky, 1405 Veterans Dr., Lexington, KY 40546-0312, USA

by which H3K27me3 is globally lost from histone-based sperm chromatin in *Arabidopsis*[5,10]. This mechanism involves silencing of H3K27me3 €writers•, the activity of H3K27me3 €erasers• and deposition of a sperm-specific histone, H3.10, which we show is immune to lysine 27 methylation. The loss of H3K27me3 facilitates transcription of genes essential for spermatogenesis and pre-configures sperm with a chromatin state that forecasts gene expression in the next generation. Thus, plants have evolved a specific mechanism to simultaneously differentiate male gametes and reprogram the paternal epigenome.

Stable inheritance of epigenetic marks during cellular proliferation is essential for maintaining cell identity and involves DNA replication-coupled mechanisms[6]. At the DNA replication fork, old histones from the mother cell are recycled and deposited onto nascent strands of daughter cell chromatin[7,8]. This mode of inheritance ensures faithful propagation of the repressive epigenetic mark H3K27me3 across cell divisions in animals[8–10]. In plants, transmission of H3K27me3-silenced states additionally involves the replication-dependent histone variant H3.1[11]. Histone H3.1 differs from H3.3 by four amino acid residues, with

these genomic data support the notion that H3.10 deposition and parental histone replacement contribute to global reprogramming of H3K27me3 in sperm.

Because *htr10* mutant plants do not show morphological or fertility defects in sperm[20], we speculated that genetically redundant mechanisms also operate to remove H3K27me3 during sperm development. Aside from histone replacement, loss of an epigenetic mark can result from a lack of specific €writers• or enhanced activity of €erasers•. We thusinvestigated the expression of methyltransferase subunits of PRC2 in *Arabidopsis*; these writers are encoded by three paralogs *€URLY LEAF (CLF), MEDEA (MEA)* and *SWINGER (SWN)*[13] - all of which were undetectable during sperm development (Fig. 1h and Extended Data Fig. 4a-c). A similar lack of expression was observed for other components of PRC2 (Extended Data Fig. 4d-g)as well as most PRC1 subunits (Extended Data Fig. 4g). The failure of SWN to accumulate after ectopic expression in sperm suggested active PRC2 turnover (Extended Data Fig. 4h). By contrast, expression of the Polycomb machinery was unaltered in egg cells (Fig. 1h and Extended Data Fig. 4g). These observations suggest that Polycomb activity is specifically compromised during spermatogenesis.

We next asked whether the loss of H3K27me3 might also involve active demethylation, as implicated in the epigenetic resetting of *FLC*[14]. Three closely related Jumonji-C family (JMJ) H3K27 demethylases -

Unlike in mammals and

accumulate H3K4me3 (Fig. 4a, cluster 3 and Supplementary Table 1) were less likely to be transcribed throughout early embryogenesis (Fig. 4b), had lower levels of expression overall (Fig. 5h) and were enriched for tissue-specific regulators of post-embryonic development

Europe PMC Funders Author Manuscripts

Extended Data

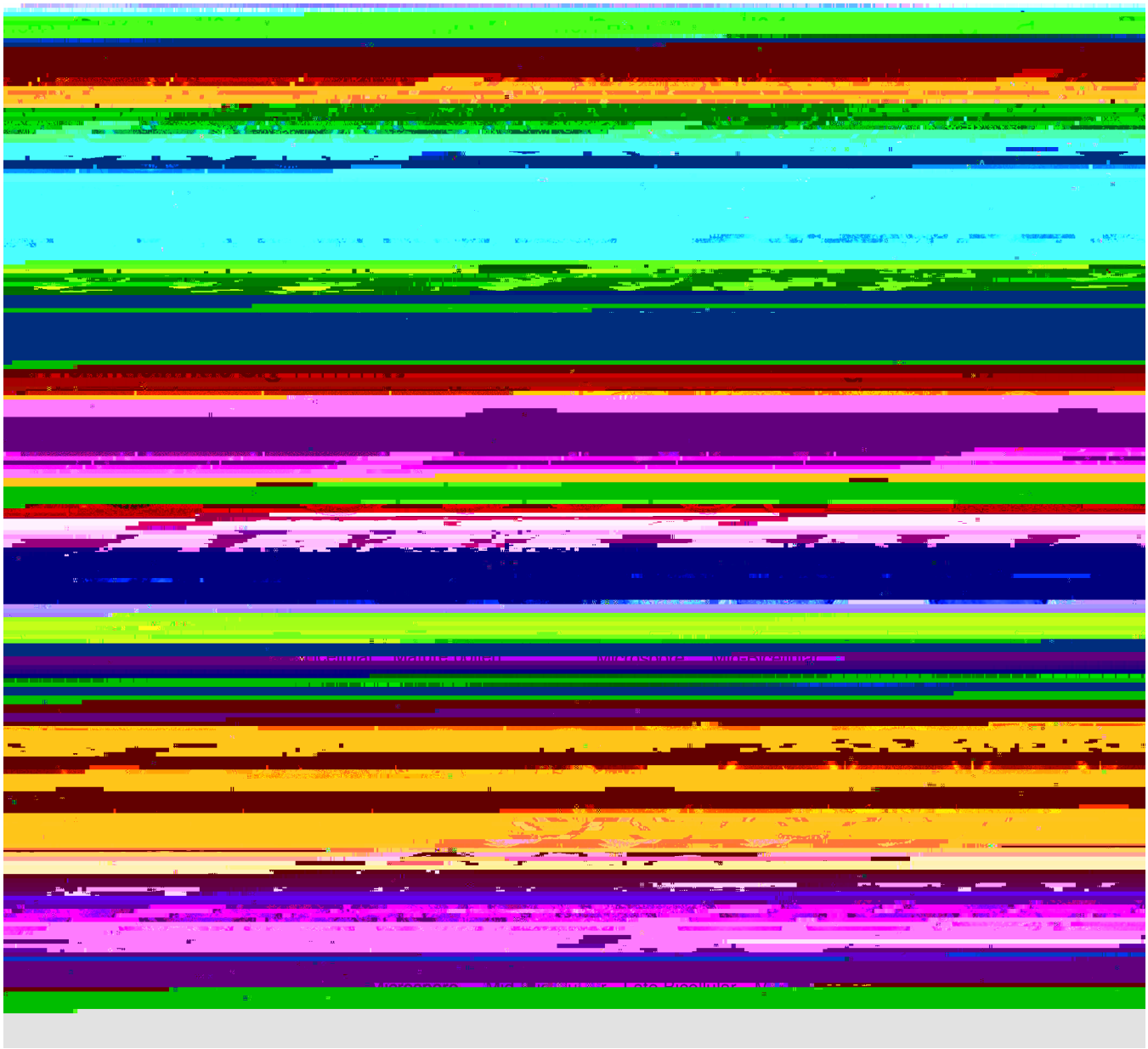

Extended Data Fig. 1.

Dynamics of histone H3.1 and H3.3 during pollen development.

Expression of H3.1 (a-d) and H3.3 (e-f) isoforms during pollen development. Histone H3.1 is encoded by five isoforms: *HTR1* (a), *HTR2* (b), *HTR3* (c), *HTR9* and *HTR13* (d). Histone H3.3 is encoded by three isoforms: *HTR4*, *HTR5* (e) and *HTR8* (f). Two pairs of genes (*HTR4-HTR5* and *HTR9-HTR13*) are found in tandem at the same locus so a single reporter for each pair was used to monitor expression. Histone H3.1 (*HTR2*, *HTR3* and *HTR13*) were detectable in the microspore and sperm precursor but this signal disappeared rapidly before sperm mitosis. No pollen expression was detected for *HTR1*. Histone H3.3 (*HTR5* and *HTR8*) were detected throughout pollen development but had a much reduced (*HTR8*) (

or absent (*HTR8*) signal in sperm. Arrows indicate expression in the microspore or VN while arrowheads distinguish expression in the sperm lineage. The marker line analysis was repeated twice with independent inflorescences. Scale, 5 μm.

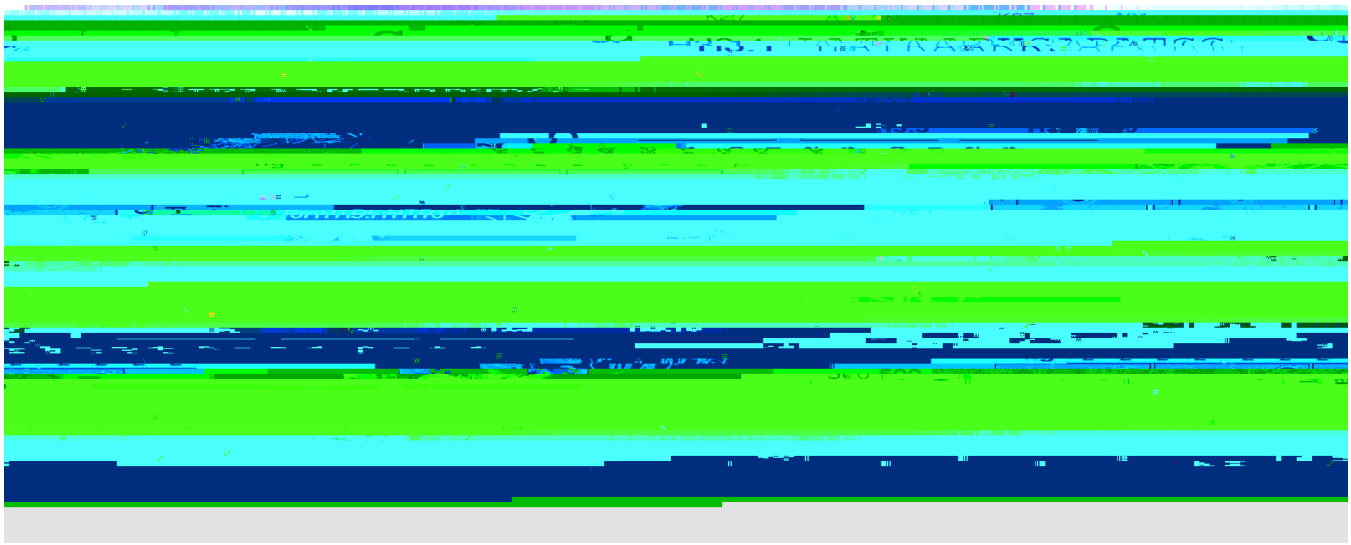

Extended Data Fig. 2.

Specificity of anti-H3K27 methylation antibodies used in this study.

a, Peptide sequences of H3.1, H3.3 and H3.10 surrounding K27 used for testing antibody specificity. Different forms with no methylation (me0), mono-methylation (me1), di-methylation (me2), and tri-methylation (me3) at K27 were used in all dot blots. **b**–**d**, Dot blots with serial dilutions of the different forms of histone H3 peptides described in **a**. The resulting membranes were probed with (**b**) H3K27me1 from Millipore #07-448 and (**c**) H3K27me3 from Millipore #07-449. Importantly, both H3K27 methylation antibodies cross react with the correct methylated form of H3.10 peptides, confirming that a lack of H3K27me3 detection in sperm chromatin (Fig. 1a) or on ectopically expressed H3.10-3xHA (Fig. 2e) is not due to poor antibody affinity. The experiment was repeated twice on two independent blots. **e**, Representative image of T1 *htr4;htr5;htr8* plants expressing either untagged H3.10 under control of an H3.3 promoter (left) or endogenous H3.3 (right). Plants devoid of endogenous H3.3 and expressing only H3.10 and H3.1 (left) were developmentally stunted and completely sterile. This was evident in two independent experiments with individual *htr4;htr5;htr8* T1 lines. Raw blots are provided in Source Data Extended data fig. 2.

Europe PMC Funders Author Manuscripts

Extended Data Fig. 3.
Epigenomic profiling of

Extended Data Fig. 4.
Dynamics of the Polycomb machinery during sperm development.
a-f, Expression of MEA-YFP (a), CFP-CLF (b), SWN-GFP (c), LHP1-YFP (d), EMF2-GFP (e) and FIE-VENUS (f) during pollen development. All markers were absent from sperm at mature pollen stage. FIE had an appreciable signal in the sperm precursor but was excluded from the nucleus. Arrows indicate expression in the microspore or VN while arrowheads distinguish expression in the sperm lineage. Marker line analysis was repeated twice with

PRC1 (bottom panel) subunits. Expression represents the inverse hyperbolic sine (asinh) transform of the mean RNA-seq TPM values obtained from previously published datasets detailed in Supplementary Table 6. Sperm and egg were profiled with three and four biological replicates, respectively. **h**, Ectopic expression of SWN-Clover under control of the sperm lineage-specific DUO1 promoter. Predicted insertions were estimated from T2 segregation of RFP fluorescent seeds arising from the pAlligatorR43 selection marker. Expression of SWN-GFP in T1 lines was barely detectable in pollen and well below that predicted from the T2 segregation data. **i**, Schematic of the action of JMJ proteins, which can demethylate H3K27 di-and tri-methylation but not mono-methylation. Statistical source data are provided in Source Data Extended data fig. 4.

Europe PMC Funders Author Manuscripts

Extended Data Fig. 5.
Transcriptional profiling of *htr10*, *elf6;ref6;jmj13* and *elf6;ref6;jmj13;htr10* pollen.
a, Principal component analysis illustrating the high reproducibility of replicates and variation among the RNA-seq datasets generated from WT (n = 3 replicates), *htr10* (n = 4 replicates), *elf6;ref6;jmj13* (n = 3 replicates) and *elf6;ref6;jmj13;htr10* (n = 3 replicates) pollen. All the biological replicates indicated (n) were used in the analysis that follows in panels b,c,d of this figure. b,c, Expression of (a) b Tj 1 /F3 -5 T.71 -2 Td [(pollH3K27 demeth) 5(yls g)] W5

Expression represents the inverse hyperbolic sine (asinh) transform of the mean RNA-seq TPM values. The mean value of the biological replicates in a is shown, while the asterisks (*) indicate significantly different expression relative to WT pollen ($p < 0.001$) using DESeq differential expression analysis and Benjamin-Hochberg correction to control for multiple comparisons. See source data for p values. d, Volcano plots summarising significantly (adjusted p-value < 0.1) up-regulated (log2 FC > 0, red) and down-regulated (log2 FC < 0, blue) genes in *htr10*, *elf6;ref6;jmj13* and *elf6;ref6;jmj13;htr10* pollen relative to WT. DESeq analysis was used to determine differentially expressed genes from the biological replicates detailed in a and multiple comparisons controlled for using Benjamin-Hochberg correction. See Supplementary Table 3. e, Differentially-expressed genes (DEGs) in *htr10* (n = 73) and *elf6;ref6;jmj13* (n = 194) significantly overlap each other. Significance of the enriched overlap (p-value) was determined using a two-sided Fisher•s exact test. f, Clustered heatmap displaying enriched gene ontology (GO) terms associated with the DEGs in *htr10* (n = 73), *elf6;ref6;jmj13* (n = 194) and *elf6;ref6;jmj13;htr10* (n = 468) pollen relative to WT. Significant enrichment was assessed using g:Profiler and controlled for the multiple testing problem using the in-built g:SCS (sets counts and sizes) correction.

a, Heatmaps centred on H3K4me3 peaks in sperm and leaf. Regions are split based on peaks being sperm-specific, leaf-specific or common to both sperm and leaf. The number of peaks and relative percentage are indicated in the labels to the left. Plotted is the ChIP$_2$-seq log

Europe PMC Funders Author Manuscripts

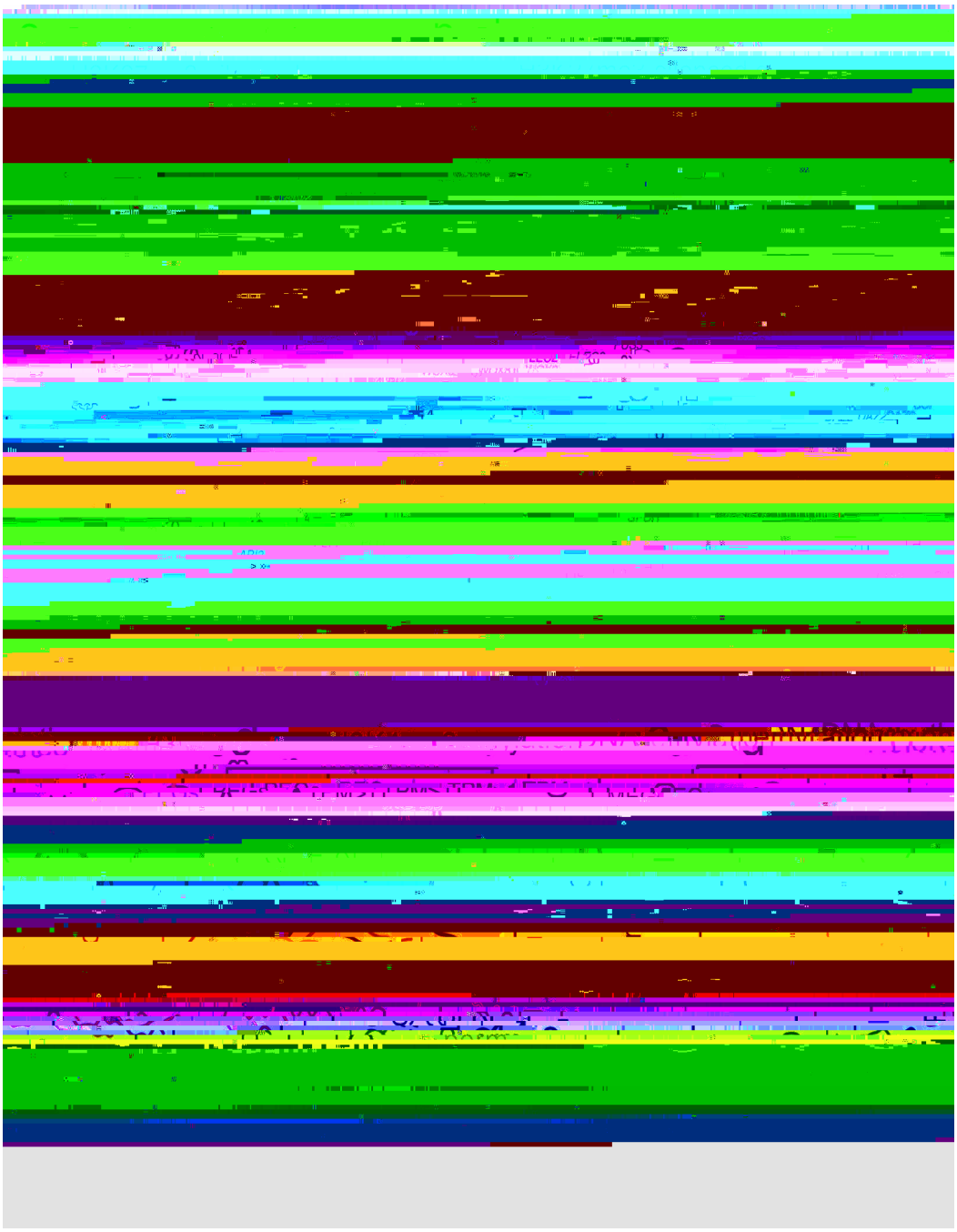

Extended Data Fig. 7.

Reprogramming of Polycomb-silenced genes in sperm.

a, Heatmap illustrating the developmentally regulated expression of somatic H3K27me3-marked genes. Expression represents z-score normalised RNA-seq TPM values. b, Heatmap of the expression of the genes marked in Figure 4a. Expression represents the inverse hyperbolic sine (asinh) transform of RNA-seq TPM values. c, Averaged DNA methylation signal over MEGs and PEGs in sperm. Plotted is the proportion of methylated cytosines in all contexts (i.e. CG, CHG and CHH). d, Averaged H3K4me3 signal over PEGs with

detectable expression (TPM>1, black line) or no expression (TPM<1, grey line) in sperm. Plotted is the ChIP-seq log2 enrichment relative to input. PEGs accumulate H3K4me3 regardless of expression in sperm, although the level of H3K4me3 enrichment was expectedly higher at sperm-expressed PEGs. Statistical source data are provided in Source Data Extended data fig. 7.

Supplementary Material

Refer to Web version on PubMed Central for supplementary material.

Acknowledgements

We thank P. Andersen and J. M. Watson for critical reading of the manuscript; Z. Lorkovic and S. Akimcheva for guidance and technical support; T. Suzuki for sequencing the egg cell transcriptome; Life Science Editors for editing services. We also thank the Vienna BioCenter Core Facilities for Next Generation Sequencing, Plant Science, HistoPathology, the IMP/IMBA BioOptics Facility and the MENDEL HPC team. This work was supported

37. Khanday I, Skinner D, Yang B, Mercier R, Sundaresan V. A male-expressed rice embryogenic trigger redirected for asexual propagation through seeds. Nature. 2019; 565:91,95. [PubMed: 30542157]
38. Horstman A, et al. The BABY BOOM Transcription Factor Activates the LEC1-ABI3-FUS3-LEC2 Network to Induce Somatic Embryogenesis. Plant Physiol. 2017; 175:848,857. [PubMed: 28830937]
39. Bosc‡ S, Knauer S, Laux T. Embryonic development in Arabidopsis thaliana: from the zygote division to the shoot meristem. Front Plant Sci. 2011; 2:93. [PubMed: 22639618]
40. Vermeulen M, et al. Selective Anchoring of TFIID to Nucleosomes by Trimethylation of Histone H3 Lysine 4. Cell. 2007; 131:58,69. [PubMed: 17884155]
41. Zhao P, Begcy K, Dresselhaus T, Sun M-X. Does Early Embryogenesis in Eudicots and Monocots Involve the Same Mechanism and Molecular Players? Plant Physiol. 2017; 173:130,142.
42. Chen J, et al. Zygotic Genome Activation Occurs Shortly after Fertilization in Maize. Plant Cell. 2017; 29:2106,2125. [PubMed: 28814645]
43. Hammoud SS, et al. Distinctive chromatin in human sperm packages genes for embryo development. Nature. 2009; 460:473,8. [PubMed: 19525931]
44. Brykczynska U, et al. Repressive and active histone methylation mark distinct promoters in human and mouse spermatozoa. Nat Struct Mol Biol. 2010; 17:679,87. [PubMed: 20473313]
45. Sachs M, et al. Bivalent Chromatin Marks Developmental Regulatory Genes in the Mouse Embryonic Germline InVivo. Cell Rep. 2013; 3:1777,1784. [PubMed: 23727241]
46. Zheng H, et al. Resetting Epigenetic Memory by Reprogramming of Histone Modifications in Mammals. Mol Cell. 2016; 63:1066,1079. [PubMed: 27635762]
47. Murphy PJ, Wu SF, James CR, Wike CL, Cairns BR. Placeholder Nucleosomes Underlie Germline-to-Embryo DNA Methylation Reprogramming. Cell. 2018; 172:993,1006.e13 [PubMed: 29456083]
48. Tabuchi TM, et al. Caenorhabditis elegans sperm carry a histone-based epigenetic memory of both spermatogenesis and oogenesis. Nat Commun. 2018; 9
49. Kaneshiro KR, Rechtsteiner A, Strome S. Sperm-inherited H3K27me3 impacts offspring transcription and development in C. elegans Nat Commun. 2019; 10:1271. [PubMed: 30894520]
50. Zenk F, et al. Germ line-inherited H3K27me3 restricts enhancer function during maternal-to-zygotic transition. Science. 2017; 357:212,216. [PubMed: 28706074]
51. Maehara K, et al. Tissue-specific expression of histone H3 variants diversified after species separation. Epigenetics Chromatin. 2015; 8:35. [PubMed: 26388943]

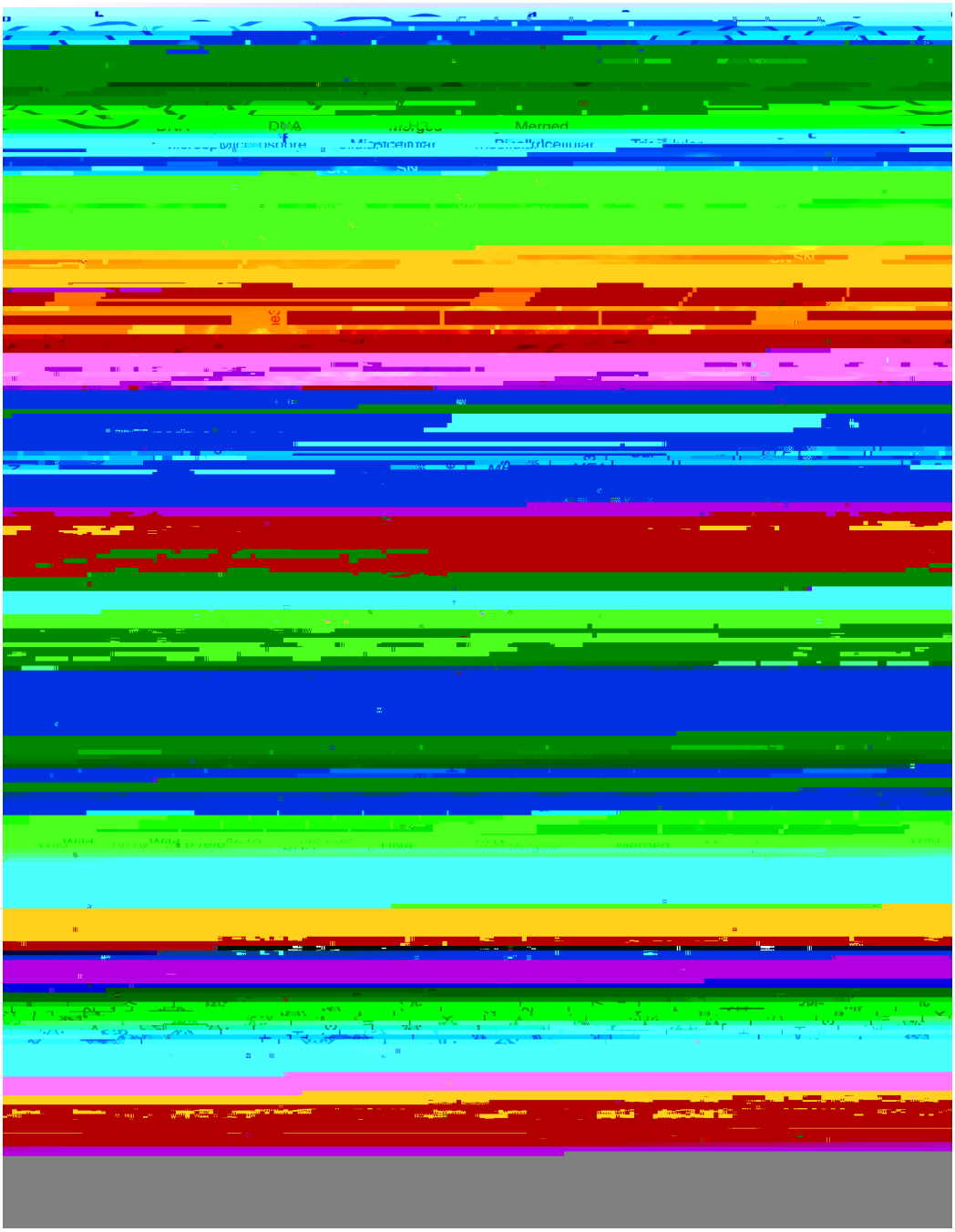

Fig. 1. H3K27me3 marks are globally lost from *Arabidopsis* sperm chromatin.
a, H3 antibody (*c*-H3) and 4′,6-diamidino-2-phenylindole (DAPI) staining of *Arabidopsis* sperm nuclei. Scale, 2 μm. b, Schematic of *Arabidopsis* pollen development. Microspore

Scale, 2 *f*m. f, Whole-mount c-H3K27me3 and DAPI staining of *Arabidopsis* pollen grains at different stages of development. Cell wall autofluorescence is indicated (cwa). Scale, 5 *f*m. The immunostaining in a and d-f was repeated twice. g, Quantification of c-H3K27me3 levels in VN and SN from WT, *htr10*, *elf6;ref6;jmj13* and *elf6;ref6;jmj13;htr10* pollen normalized to total H3 content. The violin curve represents the density of differing H3K27me3 levels. h, Expression of *Arabidopsis* histone H3 lysine 27 mono- (me1) and tri- (me3) methyltransferases (top two panels) and demethylases (third panel). Expression represents the inverse hyperbolic sine (asinh) transform of the mean RNA-seq TPM value sobtained from previously published datasets detailed in Supplementary Table 6. Sperm and egg were profiled with three and four RNA-seq biological replicates, respectively. i, c-H3K27me3 and c-H3 staining of VN and SN from wild type (WT), *elf6;ref6;jmj13* and *htr10* pollen. Scale, 2 *f*m. j, Quantification of c-H3K27me1 levels in VN and SN from WT, *htr10*, *elf6;ref6;jmj13* and *elf6;ref6;jmj13;htr10* pollen normalized to total H3 content. In g and j, red bar represents the mean of each genotype; quantification and statistical analysis were based on samples from one representative experiment; sample size (n = total number of nuclei) of each genotype is denoted alongside each violin plot. Statistical analysis was performed using a two-sided Mann-Whitney U-test. The experiment was repeated twice. Statistical source data are provided in Source Data fig. 1.

Europe PMC Funders Author Manuscripts

Fig. 2. Sperm-specific histone H3.10 is immune to K27 methylation.

a, Expression of *Arabidopsis* histone H3 variants. Expression represents the inverse hyperbolic sine (asinh) transform of the mean RNA-seq TPM values obtained from previously published datasets detailed in Supplementary Table 6. Sperm and egg were profiled with three and four biological replicates, respectively. **b**, Expression of H3.10-Clover during pollen development. Cell wall autofluorescence is indicated (cwa). The experiment was repeated twice. Scale, 5 μm. **c**, N-terminal tail alignment of histone H3.1, H3.3 and H3.10-like variants from *Arabidopsis thaliana* (AtH3.10), *Arabidopsis lyrata*

Europe PMC Funders Author Manuscripts

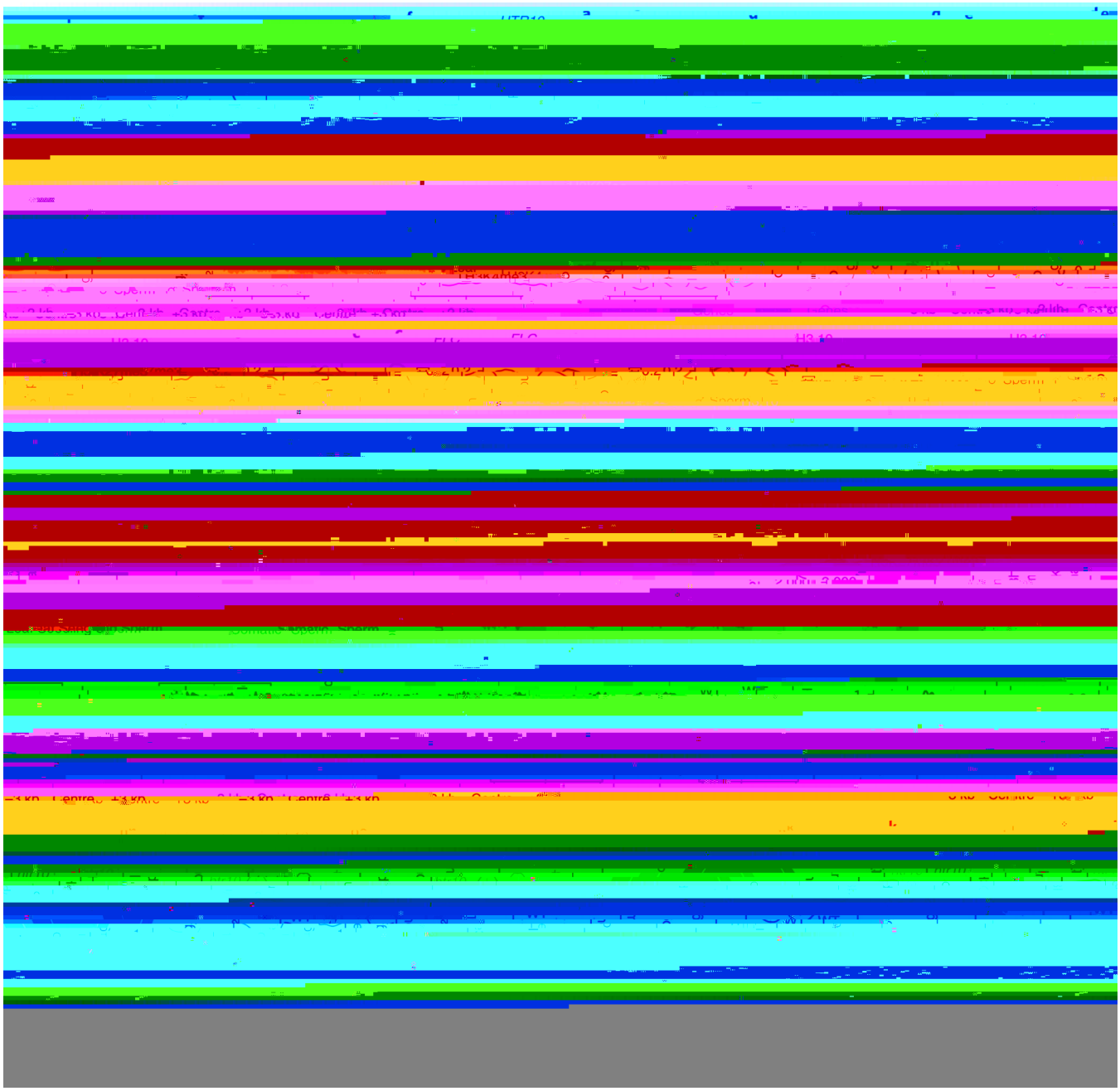

Fig. 3. H3.10 deposition in sperm correlates with the loss of H3K27me3.

a-c, ChIP-seq tracks of the region surrounding *HTR10* (a) *BBM* (b) and *FLC* (c). All three genes (blue shading) are embedded within broad somatic H3K27me3 domains. Coverage is represented as the $\log_2$ ratio of IP DNA relative to input. Coloured and grey shading indicate an enriched or depleted signal, respectively. d-f, ChIP-seq profiles of leaf H3K27me3 (top), sperm H3K27me3 (middle) and sperm H3.10 (bottom) over somatic H3K27me3 domains. In sperm, H3K27me3 is lost over these regions, which instead become enriched for H3.10. Similar profiles as shown in (d) but centered on regions enriched with H3K4me3 (e) and H3K27ac (f) in leaf. In sperm, these regions remain enriched with each mark together with

H3.10.g, Number of H3K27me3 peaks called in leaf, seedling and sperm. Somatic datasets were subsampled to read depth in sperm prior to peak calling. h, Box plot of the size distribution (in kb) of somatic and sperm H3K27me3 domains indicating the minimum and maximum values as well as the 25th, 50th and 75th quartiles. The number of peaks considered were *n*=6,235 (soma) and 478 (sperm). i, j, ChIP-seq profiles showing how H3.10 is depleted over retained H3K27me3 peaks in sperm. k–l, ChIP-seq profiles over *de novo* peaks of H3K27me1 (k) and H3K27me3 (l) in WT and *mtd1* sperm. m, ChIP-seq tracks of

maxime subsamg arepr3 10 Tf 131.45 0 T 39.4Tj /F0 n, Tf 31.6 0 Td(Box plot q prO] TJ 1 0lap86.61032

Europe PMC Funders Author Manuscripts

Fig. 4. Paternal resetting of H3K27me3 facilitates sperm specification

a, Chromatin state of Polycomb-silenced genes in leaf and sperm clustered based on sperm H3K4me3. Number of genes in is 1,866 (cluster 1), 2,220 (cluster 2) and 3,105 (cluster 3). Sperm differentiation genes (blue), embryonic factors (red) and post-embryonic regulators (grey) are marked. b, Percentage of cluster 1, 2 and 3 genes expressed in gametes, embryos and vegetative tissues (TPM > 5). TPM represents the mean obtained from previously published datasets detailed in Supplementary Table 6. Sperm and egg were profiled with three and four biological replicates, respectively. c, Sperm transcript levels (log2 RNA-seq

TPM)for genes expressed from each cluster. Sample size (n= genes with TPM > 0.1)is denoted on each boxplot, which indicates minimum and maximum values as well as 25th, 50th and 75th quartiles. Statistical analysis was performedusing a two-sided Mann-Whitney U-test.d, Percentage Polycomb targets among genes with enriched expression in sperm (n =463 genes), early embryos (n=279 genes) and early endosperm (n =463 genes)with colours corresponding to the clusters defined in panel a. Statistics is based on a one-sided permutation test (n = 100 permutations) compared with random TAIR10 regions.e, ChIP-seq tracks of three sperm differentiation genes, *SHORT SUSPENSOR (SSP), HAPLESS 2 (HAP2)* and

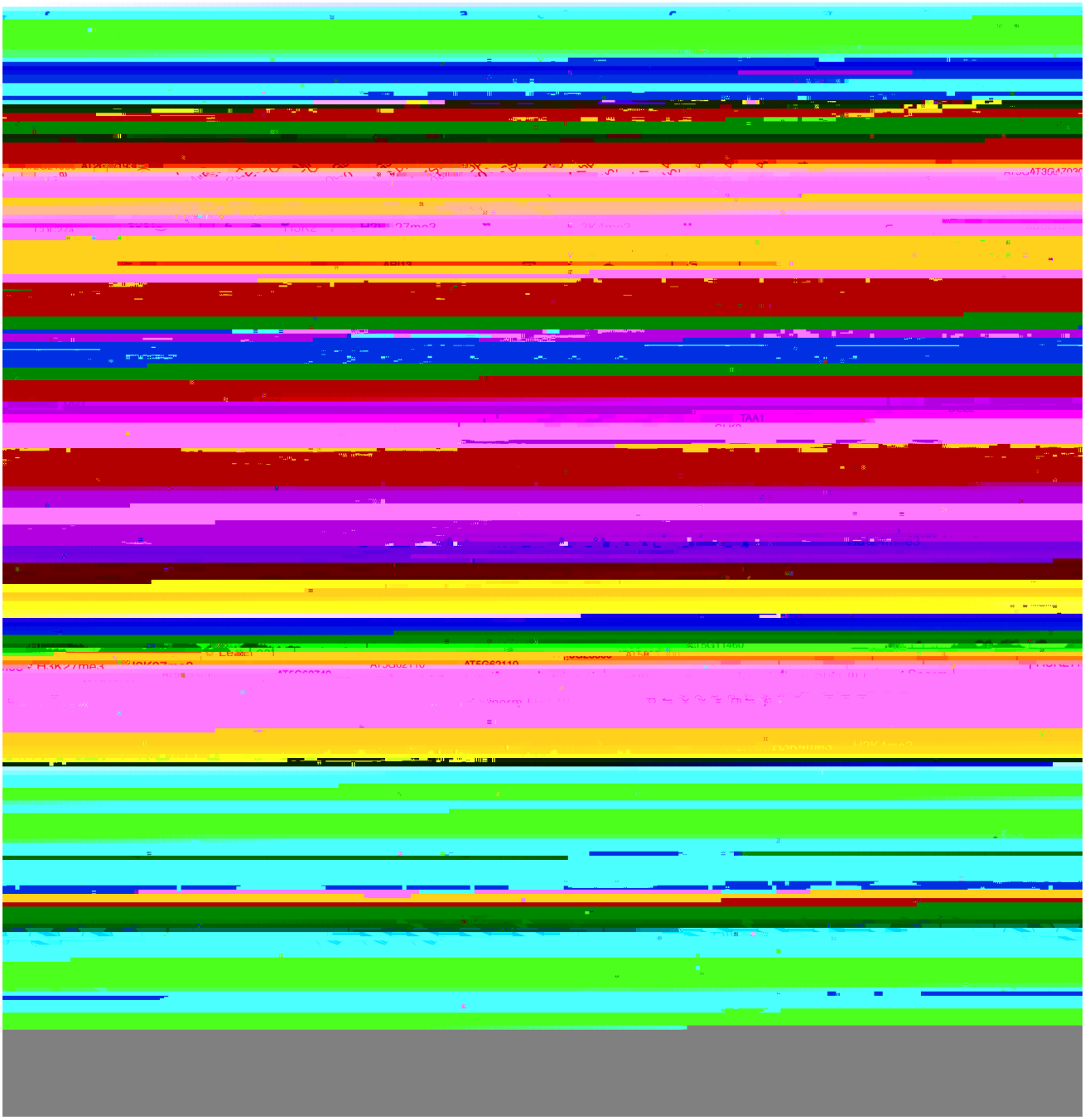

Fig. 5. Sperm chromatin state forecasts gene expression in the next generation
a, Percentage of MEGs (n = 57 genes) and PEGs (n = 66 genes) overlapping with somatic H3K27me3 domains. Significance was determined by chi-square analysis compared to proportion in *Arabidopsis* (n = 28,775 genes). b-c, H3K27me3 signal over MEGs and PEGs in leaves (b) and sperm (c). d, H3K4me3 signal over MEGs and PEGs in sperm. Plotted in c,d is the ChIP-seq log2 enrichment relative to input; b relative to H3. e, ChIP-seq tracks of three PEGs *SU(VAR)3-9 HOMOLOG 7 (SUVH7), VARIANT IN METHYLATION 5 (VIM5)*

transform of the mean RNA-seq TPM values obtained from previously published datasets detailed in Supplementary Table 6. Sperm and egg were profiled with three and four biological replicates, respectively. **y**, Overlap enrichment of paternal or maternal biased genes in early zygotes with cluster 1, 2, 3 genes. Statistical enrichment was determined using pairwise two-sided Fisher•s exact tests. See source data for sample sizes (n) and precise *p*-values. h, 14h zygote transcript levels (log_2 RNA-seq TPM) for genes expressed